

Entanglement Dynamics between Inertial and Non-uniformly Accelerated Detectors

David C. M. Ostapchuk,^{1,*} Shih-Yuin Lin,^{2,†} Robert B. Mann,^{1,‡} and B. L. Hu^{3,§}

¹*Department of Physics and Astronomy, University of Waterloo, Waterloo, Canada N2L 3G1*

²*Department of Physics, National Changhua University of Education, Changhua 50007, Taiwan*

³*Maryland Center for Fundamental Physics and Joint Quantum Institute,
University of Maryland, College Park, Maryland 20742-4111, USA*

We study the time-dependence of quantum entanglement between two Unruh-DeWitt detectors, one at rest in a Minkowski frame, the other non-uniformly accelerated in some specified way. The two detectors each couple to a scalar quantum field but do not interact directly. The primary challenge in problems involving non-uniformly accelerated detectors arises from the fact that an event horizon is absent and the Unruh temperature is ill-defined. By numerical calculation we demonstrate that the correlators of the accelerated detector in the weak coupling limit behaves like those of an oscillator in a bath of time-varying “temperature” proportional to the instantaneous proper acceleration of the detector, with oscillatory modifications due to non-adiabatic effects. We find that in this setup the acceleration of the detector in effect slows down the disentanglement process in Minkowski time due to the time dilation in that moving detector.

PACS numbers: 03.65.Ud, 03.65.Yz, 03.67.-a, 04.62.+v

I. INTRODUCTION

A uniformly accelerated, point-like observer moving in a quantum field in a Minkowski vacuum will experience the same effect as an inertial observer in a thermal field at a temperature proportional to the proper acceleration of the observer. This is called the Unruh effect [1], and the temperature experienced by the observer is called the Unruh temperature. Since the observer is uniformly accelerated and assumed to be point-like, for such an observer one can sharply define the event horizon, beyond which no information can reach the observer. The corresponding geometry is the Rindler space where all uniformly accelerated detectors follow stationary trajectories in its right wedge R. This model, first proposed by Unruh to understand the Hawking effect in a black hole, has garnered wide-spread attention on its own merit in a variety of contexts, relativistic quantum information being one of the most recent [2].

In recent years much effort has been made to understand the quantum informational aspects of the Unruh effect in various setups and for different quantum fields [3–11]. Most of the work employs arguments that rely on the existence of an event horizon. For example, one common way to show the thermality experienced by a uniformly accelerated detector on the right wedge R of the Rindler spacetime is to argue that the event horizon acts to divide the spacetime into two regions leaving one region, the left wedge L, totally inaccessible to observers in the right wedge R. Upon tracing out the field modes in L one sees easily that the observer in R experiences thermality at the Unruh temperature proportional to its proper acceleration. Nevertheless, in cases without a Rindler-like spacetime structure or the presence of an event horizon neither thermality arguments nor geometric properties are of much use. More generally, in cases where the observer undergoes non-uniform acceleration there is no timelike Killing vector nor equilibrium condition to define the Unruh temperature for all times.

The question of how a detector experiences the effects of a quantum field when it undergoes non-uniform acceleration was raised in the 90s by one of the present authors [12]: in the absence of an event horizon, will it detect radiation or not? For a purist endorsing only geometric arguments who insists on the event horizon being the determining factor, the answer would be no. But physically there is no fundamental distinction between nonuniform and uniform acceleration, and one would expect radiation, albeit not in a strictly thermal form. In fact it is natural to ask how the detector responds to a change in kinematic states, say, from an inertial state to a uniformly accelerated state, or the reverse. This is a more generic case — what one encounters in the everyday experience of driving a car to go somewhere and back. This intuitive view, though simple, is not easy to formulate, because of the non-availability of an event horizon (from the geometric viewpoint) or an equilibrium condition (from the field theory viewpoint). For a

*Electronic address: davidostapchuk@alumni.uwaterloo.ca

†Electronic address: sylin@cc.ncue.edu.tw; Corresponding author

‡Electronic address: rbmann@sciborg.uwaterloo.ca

§Electronic address: blhu@umd.edu

general trajectory one should treat the detector-quantum field system under fully nonequilibrium conditions. Using stochastic field theory (based on the influence functional representation of the quantum field, which departs from an equilibrium condition as the detector deviates from uniform acceleration), the physical predictions mentioned above (that the observer experience nonthermal radance) were confirmed [13]. Furthermore, quantum field theory in the influence functional or in-in (closed-time-path, or Schwinger-Keldysh) formulation, which is designed to treat causal evolutions (as distinct from the traditional in-out formulation for scattering problems, or imposing future dynamical conditions), liberates the physical essence of the problem from the limitations (or utility, but only when applicable) of geometric constructs such as an event horizon [37], certainly away from the gravitation and general relativity context, and attribute the Unruh effect purely as a kinematic effect related to the excitations by vacuum fluctuations by the motion of the detector in a quantum field [38]. The kinematic viewpoint and the nonequilibrium approach are clearly more encompassing and widely applicable. For example the “circular Unruh effect” [13, 14], which has been related to the Sokorov-Ternov effect observed in storage rings, can be regarded as a nonequilibrium QED effect manifest theoretically when electrons are treated as point-like objects rather than plane waves in space.

One way to study the dynamics of a non-uniformly accelerated detector is to look at the response function in the transition probability of a uniformly accelerated detector with finite coupling time to the vacuum [15–18]. One may argue that in the interaction region the detector acts like a uniformly accelerated one, while it behaves like an inertial detector in the asymptotic past, provided there is no excitation in an inertial detector initially in its ground state. Other attempts for the off-uniform acceleration cases, e.g. [19–22], are also focused on the response functions. We want to issue a note of caution here: the transition probabilities associated with these detector response functions are usually considered using time-dependent perturbation theory, which is valid only in the weak coupling (transient) limit with a nonvanishing proper acceleration [23]. Overall, for the study of entanglement dynamics of two detectors the response functions are not as convenient as the correlators, which are what we set forth to calculate below. From the correlators of two detectors traversing the full history in different states of motion, we can extract the entanglement dynamics between them.

Previous work using nonequilibrium quantum field theory (NEqQFT — for an introduction, see, e.g., [24]) concentrated primarily on the fluctuation-dissipation aspects of particles and their energy spectrum. Here we are interested in the quantum informational aspects of two non-uniformly accelerated detectors. We are specifically concerned with how quantum entanglement between these two detectors evolves in time, especially in comparison to the previously studied cases of (a) two inertial detectors [9] and (b) between one inertial detector and one uniformly accelerated detector [3–5, 10]. As a first step we therefore consider the situation in which one detector A remains at rest and a second detector B starts out from an inertial state and ends up in a uniformly accelerated state. We expect this scenario to be a hybrid nature of cases (a) and (b) above.

There is a coordinate system in Minkowski spacetime that gives a simpler description of the motion of detector B . It is given by

$$ds^2 = (e^{-2w\xi} + e^{2w\zeta})(-d\xi^2 + d\zeta^2) + dy^2 + dz^2, \quad (1)$$

which was first introduced by Kalnins [25] and later used by Costa and Villalba and others [26] for the analysis of quantum field theory of a detector undergoing non-uniform acceleration, and more recently used to study the entanglement degradation due to non-inertial motion by one of the present authors [27]. The range of the coordinates is $-\infty < (\xi, \zeta) < \infty$, which covers half of the Minkowski space (the region $x > t$.) An observer with worldline $\zeta = \zeta_0$ for some constant ζ_0 is inertial in the asymptotic past and has uniform acceleration in the asymptotic future. In this sense the coordinates (1) resemble Minkowski coordinates as $t, \xi \rightarrow -\infty$ and Rindler coordinates at $t, \xi \rightarrow +\infty$. Note that since the trajectory asymptotes to one of uniform acceleration we do have available a single event horizon, in contrast to the two horizons present for a Rindler observer.

Taking advantage of this simple description, we consider two Unruh-DeWitt (UD) detectors A and B , with A at rest in conventional Minkowski coordinates, and B accelerated non-uniformly so as to be stationary in the coordinates (1), in a quantum field initially in the Minkowski vacuum. The analysis here follows the approach of prior work by two of us on two UD detectors [9, 10]. Since the motions of the two detectors are highly asymmetric, we have to resort to numerical computation to obtain the results. Conceptually, our results demonstrate both the methods and the nature of entanglement degradation in situations without global geometric constructs such as an event horizon. From this perspective our approach provides a useful case study for comparison. In addition, our results are useful for a description of the quantum twin paradox problem [28], with the setup depicted in [12] where one tries to predict the logbook of entanglement dynamics between these two famous twins, one staying home whilst the other travels away and returns. The intellectual question is how their entanglement alters upon return in comparison to both twins staying at home, and how entanglement in the outbound trip differs from the return trip; the technical difficulty in this situation is that the returning twin does not see an event horizon.

The paper is organized as follows. In Sec. II we introduce the setup of our model. We show some selected results on the evolution of the self and cross correlators of the detectors in Secs. III A and III B, and mutual influences of

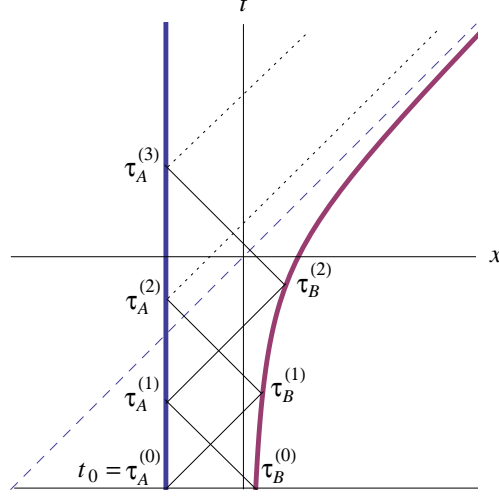


FIG. 1: The trajectories of the detectors A (left thick curve) and B (right thick curve) in the Minkowski frame. The dashed line in the plot is the event horizon for detector B . $\tau_A^{(n)}$ and $\tau_B^{(n)}$ denote the moments that the n -th order mutual influences on the detectors A and B come into play (see Section III C).

the detectors are discussed in Sec. III C. Then the entanglement dynamics between the detectors in Minkowski time will be demonstrated in Sec. III D, and a summary follows in Sec. IV. In Appendix A we give the retarded distance and the retarded time between the two detectors, and in Appendix B we include details of the numerical calculations for the self and cross correlators of the detectors. Finally in Appendix C we explain some interesting behavior of the self correlators of the non-uniformly accelerated detector during and after the transition observed in our numerical results.

II. A NON-UNIFORMLY ACCELERATED DETECTOR

Consider the dynamics of two UD detectors coupled with a quantum field. The action is given by [10]

$$S = - \int d^4x \sqrt{-g} \frac{1}{2} \partial_\mu \Phi(x) \partial^\mu \Phi(x) + \sum_{\mathbf{d}=A,B} \int d\tau_{\mathbf{d}} \left\{ \frac{m_0}{2} [(\partial_{\mathbf{d}} Q_{\mathbf{d}})^2 - \Omega_0^2 Q_{\mathbf{d}}^2] + \lambda_0 \int d^4x Q_{\mathbf{d}}(\tau_{\mathbf{d}}) \Phi(x) \delta^4(x^\mu - z_{\mathbf{d}}^\mu(\tau_{\mathbf{d}})) \right\} \quad (2)$$

where $g_{\mu\nu} = \text{diag}(-1, 1, 1, 1)$, $\partial_{\mathbf{d}} \equiv \partial/\partial\tau_{\mathbf{d}}$, Q_A and Q_B are the internal degrees of freedom of the point-like detectors A and B , assumed to be two identical harmonic oscillators with the same mass m_0 , bare natural frequency Ω_0 , and the same local time-resolution. The proper times for Q_A and Q_B are τ_A and τ_B , respectively. The scalar field Φ is assumed to be massless and λ_0 is the coupling constant. Detector A is at rest in a Minkowski frame along the world line

$$z_A^\mu = (t, -d, 0, 0) \quad (3)$$

whereas detector B moves with non-uniform acceleration, its world line given in Minkowski space by the Kalnins coordinate

$$z_B^\mu = \left(\frac{1}{a} \sinh a\xi - \frac{1}{2a} e^{-a\xi}, \frac{1}{a} \cosh a\xi - \frac{1}{2a} e^{-a\xi}, 0, 0 \right), \quad (4)$$

which is at rest at $\zeta = 0$ in the non-inertial frame (1) (see Fig. 1). From (1) with $\zeta = 0$, $d\zeta = dy = dz = 0$ and $w = a$, the proper time of detector B is related to the timelike parameter ξ by

$$ds^2 = -d\tau^2 = (e^{-2a\xi} + 1)(-d\xi^2), \quad (5)$$

so

$$\frac{d\tau}{d\xi} = \sqrt{e^{-2a\xi} + 1}, \quad (6)$$

which implies

$$\tau(\xi) = \frac{1}{a} \sinh^{-1} e^{a\xi} - \frac{1}{a} \sqrt{e^{-2a\xi} + 1} \quad (7)$$

$$= \xi + \frac{1}{a} \ln \left(1 + \sqrt{e^{-2a\xi} + 1} \right) - \frac{1}{a} \sqrt{e^{-2a\xi} + 1}. \quad (8)$$

The inverse function $\xi(\tau)$ has no closed form and has to be obtained numerically by finding the root of ξ in the above equation for a given τ . The 4-velocity and the 4-acceleration of detector B are, respectively,

$$v_B^\mu = \frac{dz_B^\mu}{d\tau} = \frac{dz_B^\mu/d\xi}{d\tau/d\xi} = \frac{1}{\sqrt{e^{-2a\xi} + 1}} \left(\cosh a\xi + \frac{e^{-a\xi}}{2}, \sinh a\xi + \frac{e^{-a\xi}}{2}, 0, 0 \right), \quad (9)$$

and

$$a_B^\mu = \frac{dv_B^\mu}{d\tau} = \left(\frac{ae^{a\xi}}{2(e^{-2a\xi} + 1)^2}, \frac{a(e^{a\xi} + 2e^{-a\xi})}{2(e^{-2a\xi} + 1)^2}, 0, 0 \right). \quad (10)$$

So the proper acceleration of the accelerated detector B reads

$$\alpha_B \equiv \sqrt{a_{B\mu} a_B^\mu} = \frac{a}{(e^{-2a\xi} + 1)^{3/2}}, \quad (11)$$

which approaches zero at the initial moment $t_0 \ll -1$ ($\xi \rightarrow -\infty$), increases to $a/2$ at $t \approx -0.114/a$ ($e^{-2a\xi} = 2^{2/3} - 1$), and then to a as $t \gg 1$ ($\xi \rightarrow \infty$).

We pause to note that the non-adiabatic behaviour of the response functions of a single non-uniformly accelerated detector has been previously considered by expanding in powers of \dot{a}/a^2 [22]. Unfortunately such analysis is not practical here because our detector B has $\dot{\alpha}_B/\alpha_B^2 = 3e^{-2a\xi(\tau)}$, which is much greater than 1 through the early stage of evolution (when $\xi(\tau)$ is negatively large and α_B is almost zero), but not that large as the proper acceleration undergoes a transition from approximately 0 to a around $t \approx 0$. It would be interesting to look at the dynamics of a detector having a transition from one non-zero proper acceleration to another in order to appropriately compare our results with these earlier ones in [22]. However, this would divert the focus of the present paper, which is concerned with the dynamics of entanglement between an inertial and a non-uniformly accelerated detector. Suffice it to note that the authors of [22] observed that the behaviour of the response functions with $a \gg \Omega$ is qualitatively different from those with $a \ll \Omega$. We observe similar behaviour of the self correlators of detector B .

III. ENTANGLEMENT DYNAMICS AND DETECTOR CORRELATORS

We consider a situation in which the initial state at $t = t_0$ in the Minkowski frame is a product state of the Minkowski vacuum of the field $|0_M\rangle$ (which is Gaussian) and the Gaussian two-mode squeezed state [9]

$$\rho_{AB}(Q_A, P_A, Q_B, P_B) = \frac{1}{\pi^2 \hbar^2} \exp -\frac{1}{2} \left[\frac{\beta^2}{\hbar^2} (Q_A + Q_B)^2 + \frac{1}{\alpha^2} (Q_A - Q_B)^2 + \frac{\alpha^2}{\hbar^2} (P_A - P_B)^2 + \frac{1}{\beta^2} (P_A + P_B)^2 \right] \quad (12)$$

of the detectors in Wigner representation. At $t = t_0$, the detectors start to couple with the quantum field. By virtue of the linearity of the combined system (2), the quantum state of the combined system, and therefore the reduced state of the detectors, will always be Gaussian and fully determined by the covariance matrix

$$\mathbf{V} = \begin{pmatrix} \mathbf{v}_{AA} & \mathbf{v}_{AB} \\ \mathbf{v}_{BA} & \mathbf{v}_{BB} \end{pmatrix} \quad (13)$$

in which the elements of the 2×2 matrices \mathbf{v}_{ij} , $i, j = A, B$ are those symmetrized two-point correlators $\mathbf{v}_{ij}^{mn} = \langle \mathcal{R}_i^m, \mathcal{R}_j^n \rangle \equiv \langle (\mathcal{R}_i^m \mathcal{R}_j^n + \mathcal{R}_j^n \mathcal{R}_i^m) \rangle / 2$ with $\mathcal{R}_i^m = (Q_i(t), P_i(t))$, $m, n = 1, 2$. We thus have full information of the reduced state of the detector pair at each moment once we know the history of all the two-point correlators, from which the dynamics of entanglement between the detectors can be extracted.

Also, by virtue of linearity, the operators of the detectors in the Heisenberg picture will evolve to a linear combination of all the detector operators $\hat{Q}_{\mathbf{d}}$, $\hat{P}_{\mathbf{d}}$ ($\mathbf{d} = A, B$) and the field operators $\hat{\Phi}_{\mathbf{k}}$, $\hat{\Pi}_{\mathbf{k}}$ defined at the initial moment t_0 as

$$\hat{Q}_{\mathbf{d}}(\tau_{\mathbf{d}}) = \hat{Q}_{\mathbf{d}}^{\mathbf{D}}(\tau_{\mathbf{d}}) + \hat{Q}_{\mathbf{d}}^{\mathbf{F}}(\tau_{\mathbf{d}}), \quad (14)$$

where $\hat{Q}_d^D(\tau_d) \equiv \sum_{d'=A,B} [\phi_{d'}^d(\tau_d) \hat{Q}_{d'} + \pi_{d'}^d(\tau_d) \hat{P}_{d'}]$ and $\hat{Q}_d^F(\tau_d) \equiv \int \frac{d^3k}{(2\pi)^3} [\phi_d^k(\tau_d) \hat{\Phi}_k + \pi_d^k(\tau_d) \hat{\Pi}_k]$. Here $\phi_d(\tau_d)$, $\pi_d(\tau_d)$ are mode functions, and we have $\hat{P}_d(\tau_d) = m_0 \partial_d \hat{Q}_d(\tau_d)$ from (2). Then each symmetrized two-point correlator of the detectors will split into a sum of the a-part and the v-part [29] as

$$\langle \mathcal{R}_d(\tau_d), \mathcal{R}'_{d'}(\tau_{d'}) \rangle = \langle \mathcal{R}_d(\tau_d), \mathcal{R}'_{d'}(\tau_{d'}) \rangle_a + \langle \mathcal{R}_d(\tau_d), \mathcal{R}'_{d'}(\tau_{d'}) \rangle_v, \quad (15)$$

with $\mathcal{R}, \mathcal{R}' = P, Q$ and

$$\langle \mathcal{R}_d(\tau_d), \mathcal{R}'_{d'}(\tau_{d'}) \rangle_a \equiv \frac{1}{2} \text{Tr} \left[\left(\mathcal{R}_d^D(\tau_d) \mathcal{R}'_{d'}^D(\tau_{d'}) + \mathcal{R}'_{d'}^D(\tau_{d'}) \mathcal{R}_d^D(\tau_d) \right) \rho_{AB} \right], \quad (16)$$

$$\langle \mathcal{R}_d(\tau_d), \mathcal{R}'_{d'}(\tau_{d'}) \rangle_v \equiv \frac{1}{2} \langle 0_M | (\mathcal{R}_d^F(\tau_d) \mathcal{R}'_{d'}^F(\tau_{d'}) + \mathcal{R}'_{d'}^F(\tau_{d'}) \mathcal{R}_d^F(\tau_d)) | 0_M \rangle. \quad (17)$$

The a-part corresponds to the initial state of the detector (12), while the v-part corresponds to the response to the field vacuum $|0_M\rangle$. The a-parts of the correlators are relatively easy to obtain in the perturbative regime with large distance between the detectors. Some examples will be given in Sec. III D. The calculation of the v-parts, however, is more complicated. Unlike detectors in uniform acceleration, there is no simple symmetry here to help in obtaining analytic results. All of our computations will be performed numerically, even in the weak-coupling regime with mutual influences neglected.

A. Dynamics of Single detectors

The reduced state of a single detector is obtained by tracing out the other detector in the reduced state of the detector pair. Since the latter is Gaussian, the former must also be a Gaussian state, which is fully determined by the self correlators of that detector.

Neglecting mutual influences between the two detectors, the self correlators of the inertial detector A have previously been obtained in closed form [23]. For the accelerated detector B , unfortunately, there is no analytic expression for its self correlators. The v-part of the latter can be expressed in 2D integrals as, for example,

$$\langle Q_B(\tau), Q_B(\tau') \rangle_v = \frac{\lambda_0^2}{m_0^2 \Omega^2} \text{Re} \int_{\tau_0}^{\tau} d\tilde{\tau} \int_{\tau_0}^{\tau'} d\tilde{\tau}' K(\tau - \tilde{\tau}) K(\tau - \tilde{\tau}') D^+(z_B^\mu(\tilde{\tau}), z_B^\mu(\tilde{\tau}')), \quad (18)$$

where $\tau, \tau' \geq \tau_0 \equiv \tau(t_0)$, $K(x) \equiv e^{-\gamma x} \sin \Omega x$ with the coupling strength $\gamma \equiv \lambda_0^2 / 8\pi m_0$ and the renormalized natural frequency Ω of the detector (see Eq. (3.59) in Ref. [30] and Eq.(59) in [29], where the τ in $q^{(-)}$ should be τ'), and

$$D^+(z_B^\mu(\tilde{\tau}), z_B^\mu(\tilde{\tau}')) = \frac{\hbar / (2\pi)^2}{|\mathbf{z}_B(\tilde{\tau} - (i\epsilon/2)) - \mathbf{z}_B(\tilde{\tau}' + (i\epsilon/2))|^2 - [z_B^0(\tilde{\tau} - (i\epsilon/2)) - z_B^0(\tilde{\tau}' + (i\epsilon/2))]^2} \quad (19)$$

is the positive frequency Wightman function of the massless scalar field. (Note that (19) is not exactly the same as the one in Eq.(3.59) in Ref. [30]. The latter can yield unphysical results. See Refs. [19, 20] and Appendix A.1 in [11] for more details.) The above integrand is singular at $\tilde{\tau} = \tilde{\tau}'$ if $\epsilon = 0$. To treat this singularity properly we calculate the quantity

$$\begin{aligned} \delta \langle Q_B^2(\tau) \rangle_v &\equiv \lim_{\tau' \rightarrow \tau} \left[\langle Q_B(\tau), Q_B(\tau') \rangle_v - \langle Q_B(\tau), Q_B(\tau') \rangle_{v(a \rightarrow 0)} \right] \\ &= \frac{2\gamma\hbar}{\pi m_0 \Omega^2} \int_{\tau_0}^{\tau} d\tilde{\tau} \int_{\tau_0}^{\tau} d\tilde{\tau}' K(\tau - \tilde{\tau}) K(\tau - \tilde{\tau}') \tilde{f}(\tilde{\tau}, \tilde{\tau}') \end{aligned} \quad (20)$$

instead, where

$$\tilde{f}(\tilde{\tau}, \tilde{\tau}') \equiv -\frac{a^2}{4(1 + e^{-a[\xi(\tilde{\tau}) + \xi(\tilde{\tau}')]}) \sinh^2 \frac{a}{2} [\xi(\tilde{\tau}) - \xi(\tilde{\tau}')] } + \frac{1}{(\tilde{\tau} - \tilde{\tau}')^2} \quad (21)$$

(with ϵ neglected). This is the deviation from $\langle Q_B(\tau) Q_B(\tau') \rangle_{v(a \rightarrow 0)}$ for inertial detectors in the Minkowski vacuum, namely, the one for detector A (Eq. (A9) in [23]) with t replaced by τ .

Now the integrand of (20) is regular and well controlled because the divergences in the coincidence limit $\tau' \rightarrow \tau$ of this theory (corresponding to the large constants Λ_1 and Λ_0 defined in Ref. [23], which are reference frame independent since they are defined via the proper times of the detectors) all belong to $\langle Q_B^2(\tau) \rangle_{v(a \rightarrow 0)}$. Indeed, it is straightforward

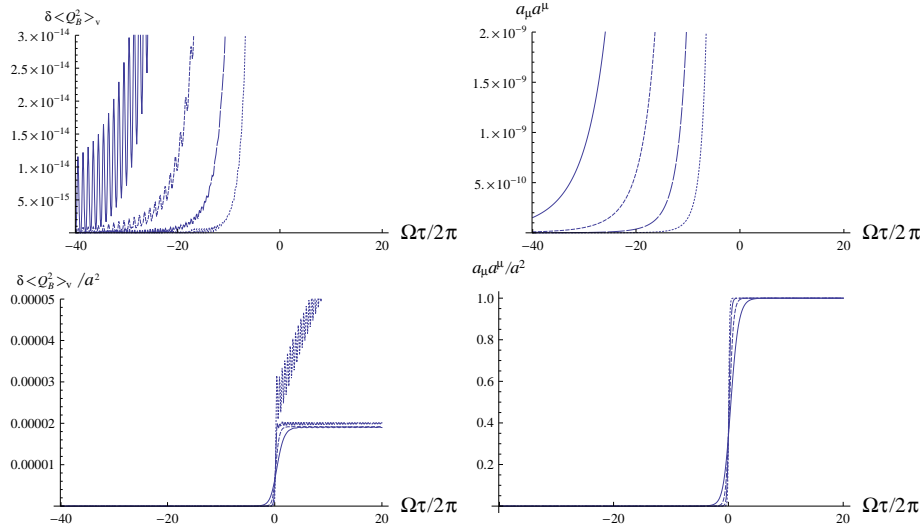


FIG. 2: Here we take $\gamma = 0.01$, $\Omega = 2.3$, and $m_0 = \hbar = 1$. The curves in these plots are those with $a = 1/4$ (solid), $1/2$ (short-dashed), 1 (long-dashed), and 2 (dotted), respectively. (Upper-left) The early evolution of $\delta \langle Q_B^2(\tau) \rangle_v$, whose growth rate is quite similar to the corresponding $\alpha_B^2 = a_\mu a^\mu$ (upper-right). The oscillations at early times are artifacts caused by the impulse at the initial moment τ_0 ; they should vanish as $\tau_0 \rightarrow -\infty$ when the proper acceleration is exactly zero. (Lower-left) Evolution of $\delta \langle Q_B^2(\tau) \rangle_v$ normalized by a^2 . All curves with $a \leq 1$ behave similarly to $\alpha_B^2(\tau)$ (lower-right), with the small oscillations mainly due to the initial impact at $\tau = \tau_0 = -80\pi/\Omega$. The oscillations in the curves with $a = 2$ are due to a non-adiabatic effect associated with the small time scale of the rapid growth in acceleration. Note that here the height of the “jump” divided by a^2 around $\tau = 0$ is $\gamma/[6\pi(\gamma^2 + \Omega^2)^2] \approx 1.896 \times 10^{-5}$ (cf. (22) with $\hbar = m_0 = 1$).

to verify that the terms in the curly bracket go smoothly to $(1/12)a_\mu(\xi(T))a^\mu(\xi(T)) + O(\tilde{\tau} - \tilde{\tau}')$, which is regular as $\tilde{\tau} - \tilde{\tau}' \rightarrow 0$. Here $T \equiv (\tilde{\tau} + \tilde{\tau}')/2$, and the proper acceleration $\alpha_B(T) = \sqrt{a_\mu(\xi(T))a^\mu(\xi(T))}$ has been given in (11).

The above integrand is suppressed rapidly when T becomes more and more negative, meaning that the value of the correlator $\langle Q_B^2(\tau) \rangle_v$ will be very close to the value of $\langle Q_B^2(\tau) \rangle_{v(a \rightarrow 0)}$ at $\Omega\tau \ll -1$, when the detector is almost at rest in Minkowski frame. After $T \gtrsim 0$, the absolute value of the integrand becomes significant around $\tilde{\tau} = \tilde{\tau}'$, so the difference $\delta \langle Q_B^2(\tau) \rangle_v$ becomes obvious after τ becomes positive.

We show some results in Fig. 2 (more details on numerical calculations can be found in Appendix B). From the lower-left plot of Fig. 2 one can see that the value of $\delta \langle Q_B^2 \rangle_v$ has a “jump” around $\tau \approx 0$ when the proper acceleration significantly departs from zero. This jump is in fact adiabatic: compared with the lower-right plot of Fig. 2, the increasing rate of $\delta \langle Q_B^2 \rangle_v$ during the jump is virtually the same as the growth rate of α_B^2 . From these numerical results we observed that the jump around $\tau \approx 0$ is from 0 to a value about

$$\mathcal{Q} \equiv \frac{\gamma \hbar a^2}{6\pi m_0 (\gamma^2 + \Omega^2)^2}. \quad (22)$$

A discussion on this observation is given in Appendix C. Note that the difference of the asymptotic values of the two-point functions reads

$$\langle Q_B^2(\infty) \rangle_v - \langle Q_B^2(-\infty) \rangle_v = \frac{\hbar}{2\pi m_0 \Omega} \left\{ \text{Re} \left[\frac{ia}{\gamma + i\Omega} - 2i\psi \left(1 + \frac{\gamma + i\Omega}{a} \right) \right] - i \ln \frac{\gamma - i\Omega}{\gamma + i\Omega} \right\} \quad (23)$$

$$\approx \frac{\hbar}{2\pi m_0} \frac{\gamma a^2}{3(\gamma^2 + \Omega^2)^2} + O(a^4), \quad (24)$$

from Eqs. (A7) and (A11) in [23], where $\psi(x)$ is the digamma function. Interestingly enough, the $O(a^2)$ term in (24) is identical to \mathcal{Q} , which is always less than the value of the left hand side of (24).

After the jump ($\tau \gtrsim 0$), we observe that those values of $\delta \langle Q_B^2 \rangle_v$ keep growing roughly as

$$\delta \langle Q_B^2(\tau) \rangle_v \sim [\langle Q_B^2(+\infty) \rangle_v - \langle Q_B^2(-\infty) \rangle_v] (1 - e^{-2\gamma\tau}) + \mathcal{Q}e^{-2\gamma\tau} \quad (25)$$

in the weak coupling limit. This is similar to the behavior of a harmonic oscillator in contact with a “thermal” bath at a time-varying “temperature”.

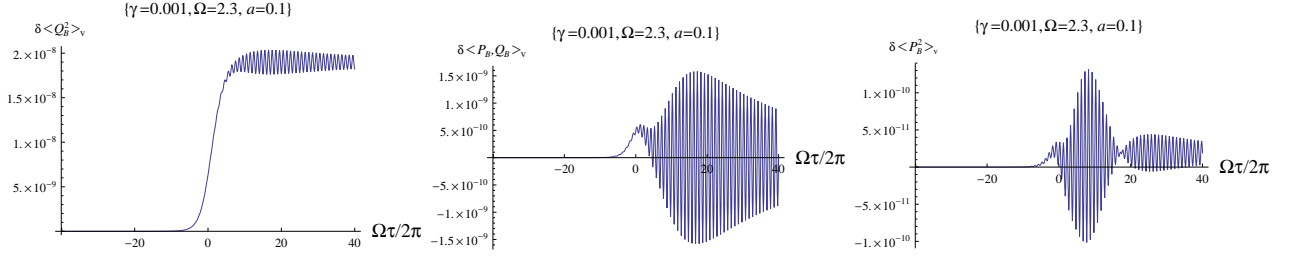


FIG. 3: Evolution of $\delta \langle Q_B^2(\tau) \rangle_v$ (left), $\delta \langle P_B, Q_B(\tau) \rangle_v$ (middle), and $\delta \langle P_B^2(\tau) \rangle_v$ (right) in proper time τ of detector B with a small a and a weaker γ . Here $\gamma = 0.001$, $\Omega = 2.3$, $m_0 = \hbar = 1$, and $a = 0.1 < 1$. The oscillations here are mainly produced by the impulse at the initial moment and can be suppressed by choosing a more negative initial moment or a smaller a .

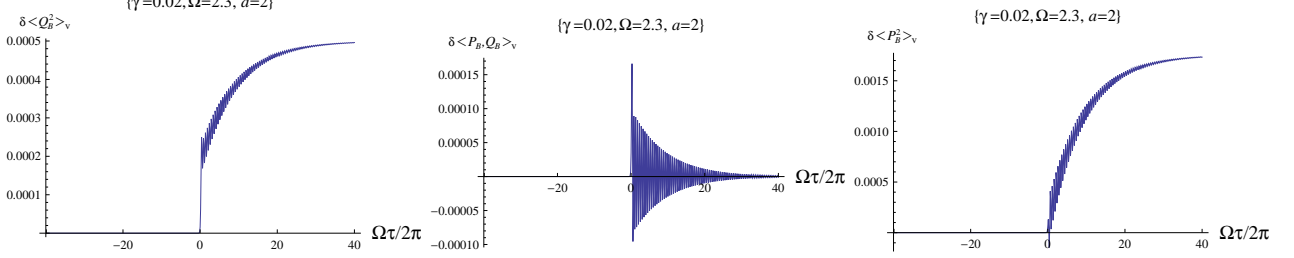


FIG. 4: Evolution of $\delta \langle Q_B^2(\tau) \rangle_v$ (left), $\delta \langle P_B, Q_B(\tau) \rangle_v$ (middle), and $\delta \langle P_B^2(\tau) \rangle_v$ (right) in proper time τ of detector B with a large late-time proper acceleration a . Here $\gamma = 0.02$, $\Omega = 2.3$, $m_0 = \hbar = 1$, and $a = 2 > 1$. The oscillations here are due to a non-adiabatic effect during the transition and cannot be suppressed by choosing a more negative initial moment.

In those cases with small a ($a \lesssim \Omega/\pi$ here), the oscillations on top of the growth curves of $\delta \langle Q_B^2(\tau) \rangle_v$ are mainly due to the impulse at the initial moment (see Figs. 2 (upper-left) and 3 (left)). One can see this by observing that (11) implies the proper acceleration $\alpha_B(\tau) \approx a e^{-3a|\tau|}$ when $a\tau \ll -1$ (as shown in the upper-right plot of Fig. 2). Indeed, these oscillations (in the cases with $a \lesssim 0.73$) will be reduced if we choose a more negative initial moment τ_0 or a larger a (Fig. 2 (upper-left)) to suppress the initial value of the proper acceleration $\alpha_B(\tau_0)$. However, in those cases with larger late-time proper accelerations ($a \gtrsim \Omega/\pi$), though the impulse at the initial moment is more suppressed, the amplitudes of those oscillations after $\tau \approx 0$ become even larger but almost independent of the initial moment τ_0 for $\Omega\tau_0 \ll -1$; this is illustrated in our numerical results in Fig. 2 (lower-left) and Fig. 4 (left). This indicates that these oscillations are coming from the non-adiabatic growth of the proper acceleration around $\tau = 0$ rather than the initial impulse.

To see the non-adiabatic behavior more closely, we set $\chi \equiv a\xi(\tilde{\tau})$ and $\chi' \equiv a\xi(\tilde{\tau}')$, and rewrite the $\tilde{\tau}$ -integrals into the χ -integrals. Eq. (20) then becomes

$$\delta \langle Q_B^2(\tau) \rangle_v = \frac{2\gamma\hbar}{\pi m_0 \Omega^2} \int_{a\xi(\tau_0)}^{a\xi(\tau)} d\chi \int_{a\xi(\tau_0)}^{a\xi(\tau)} d\chi' K(\tau - \tau(\chi/a)) K(\tau - \tau(\chi'/a)) f(\chi, \chi'), \quad (26)$$

where

$$f(\chi, \chi') \equiv \sqrt{e^{-2\chi} + 1} \sqrt{e^{-2\chi'} + 1} \left\{ \frac{-1}{4(1 + e^{-(\chi+\chi')}) \sinh^2\left(\frac{\chi-\chi'}{2}\right)} + \frac{1}{a^2 [\tau(\chi/a) - \tau(\chi'/a)]^2} \right\}. \quad (27)$$

Here $\tau(\xi)$ was given in (8), implying that f is actually independent of a in terms of χ and χ' . Now all the dependence on a in (26) is coming from the K functions as well as the upper and the lower limits of the integration. In Appendix C we can see that the length scale of the non-trivial structure of the function f in $\chi\chi'$ -space is roughly of order 1 (see Figure 12), while the length scale of oscillations of K in χ is about $a\pi/\Omega$ for $\chi \gtrsim 0$. Thus for $a \ll \Omega/\pi$, K oscillates so rapidly that the structure of f will be averaged out after integration. so $\delta \langle Q_B^2(\tau) \rangle_v$ evolves smoothly, whereas for $a \gtrsim \Omega/\pi$, the structure of f could induce significant non-adiabatic oscillations of $\delta \langle Q_B^2(\tau) \rangle_v$.

Similar quantities for the v-parts of other self correlators of detector B can be obtained by replacing $K(x)$ by $K'(x) = dK(x)/dx$ whenever $Q_B(\tau(t))$ is replaced by $P_B(\tau(t))$ in (20). Two examples are shown in Figs. 3 and 4. One can see that $\delta \langle P_B^2(\tau) \rangle_v$ behaves roughly similar to $\delta \langle Q_B^2(\tau) \rangle_v$, except for the larger oscillations and the lack of a significant jump around the transition time $\tau \approx 0$, while $\delta \langle Q_B(\tau), P_B(\tau) \rangle_v$ is manifest only after $\tau \approx 0$.

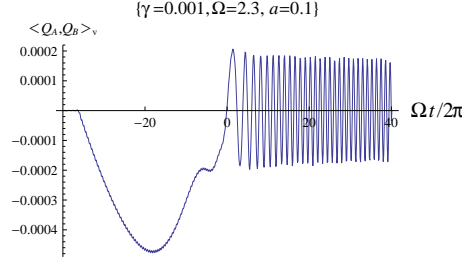


FIG. 5: Numerical results for the cross correlator $\langle Q_A(t), Q_B(\tau(t)) \rangle_v$ with $d = 10$ evolving in Minkowski time t . Other cross correlators $\langle Q_A, P_B \rangle_v$, $\langle P_A, Q_B \rangle_v$, and $\langle P_A, P_B \rangle_v$ have similar behaviors.

B. Cross correlators in Minkowski Time

From (3) and (4), we have

$$\begin{aligned} & \langle Q_A(t), Q_B(\tau(t)) \rangle_v^{(0)} \\ &= \frac{2\gamma\hbar}{\pi m_0 \Omega^2} \text{Re} \int_{t_0}^t d\tilde{\tau} \int_{\tau(t_0)}^{\tau(t)} d\tilde{\tau}' \frac{K(t - \tilde{\tau})K(\tau(t) - \tilde{\tau}')}{\left[-d - \frac{1}{a} \cosh a\tilde{\xi}' + \frac{1}{2a} e^{-a\tilde{\xi}'}\right]^2 - \left[\tilde{\tau} - \frac{1}{a} \sinh a\tilde{\xi}' + \frac{1}{2a} e^{-a\tilde{\xi}'} - i\epsilon\right]^2} \\ &= \frac{2\gamma\hbar}{\pi m_0 \Omega^2} \text{Re} \int_{t_0}^t d\tilde{\tau} \int_{\tau(t_0)}^{\tau(t)} d\tilde{\tau}' \frac{K(t - \tilde{\tau})K(\tau(t) - \tilde{\tau}')}{2d + a^{-1}e^{a\tilde{\xi}'}} \left[\frac{1}{\tilde{\tau} + d + a^{-1}e^{-a\tilde{\xi}'} - i\epsilon} - \frac{1}{\tilde{\tau} - d - 2a^{-1} \cosh a\tilde{\xi}' - i\epsilon} \right], \quad (28) \end{aligned}$$

with $\tilde{\xi}' \equiv \xi(\tilde{\tau}' + i\epsilon)$. The v-parts of other cross correlators can be obtained by replacing $K(t - \tilde{\tau})$ by $K'(t - \tilde{\tau})$ whenever $Q_A(t)$ is replaced by $P_A(t)$, and replacing $K(\tau(t) - \tilde{\tau}')$ by $K'(\tau(t) - \tilde{\tau}')$ whenever $Q_B(\tau(t))$ is replaced by $P_B(\tau(t))$. An example of the cross correlators is shown in Fig. 5. One can see that the early-time behavior of the cross correlators in this setup is quite similar to those of two inertial detectors [9] (see also Fig. 11). The absolute values of the cross correlators start to grow significantly after each detector enters the other's light cone, then keep growing until the motion of detector B becomes obvious. After $t \approx 0$, the behavior of the cross correlators turns to a fashion similar to those in the case of uniformly accelerated detectors [10, 11]. They become oscillating in t with amplitude decaying as $e^{-2\gamma t}$.

Comparing the results in Fig. 5 and Fig. 3 with the same parameters ($\gamma = 0.001$, $\Omega = 2.3$, $a = 0.1$), we find that even for $d = 10$, which is not very small, the values of the v-part of the cross correlators in this parameter regime are much greater than those of the deviations of the v-part of the self correlators from their zero-acceleration limits.

C. Mutual influences

From the equations of motion for the mode functions Eqs. (13)–(16) in [10], the mode functions with corrections from mutual influences can be written as

$$q_j^{(\mu)} = q_j^{(\mu)(0)} + \sum_{n=1}^{\infty} q_j^{(\mu)(n)}, \quad (29)$$

where $q_j^{(\mu)(0)}$ are the zeroth order solutions without considering mutual influences, and

$$q_j^{(\mu)(n)}(\tau) = \frac{2\gamma}{\Omega} \int_{\tau_0}^{\tau} d\tilde{\tau} \theta(\tau - \tilde{\tau}) \left(\tau_j^{ret}(\tilde{\tau}) - \tau_j^{(n-1)} \right) K(\tau - \tilde{\tau}) \frac{q_j^{(\mu)(n-1)}(\tau_j^{ret}(\tilde{\tau}))}{R_{j \rightarrow j}(\tilde{\tau})} \quad (30)$$

with $\mu \in \{A, B, +, -\}$, $i, j \in \{A, B\}$, $\bar{A} \equiv B$, $\bar{B} \equiv A$, the retarded times $\tau_A^{ret}(\tilde{\tau}) = t^{ret}(z_B^\mu(\tilde{\tau}))$ and $\tau_B^{ret}(\tilde{\tau}) = \tau(\xi^{ret}(z_A^\mu(\tilde{\tau})))$, $\tau_j^{(n)} \equiv [\tau_j^{ret}]^{-1}(\tau_j^{(n-1)})$, $\tau_A^{(0)} \equiv t_0$, $\tau_B^{(0)} \equiv \tau(\xi(t_0))$, and the retarded distance $R_{j \rightarrow j}$ defined in Appendix A (see Fig. 1).

For the a-part of the correlators, it is straightforward to obtain the corrected results by simply inserting the corresponding (29) into Eq. (25) in [10]. For the v-part of the correlators, the calculation is not as straightforward

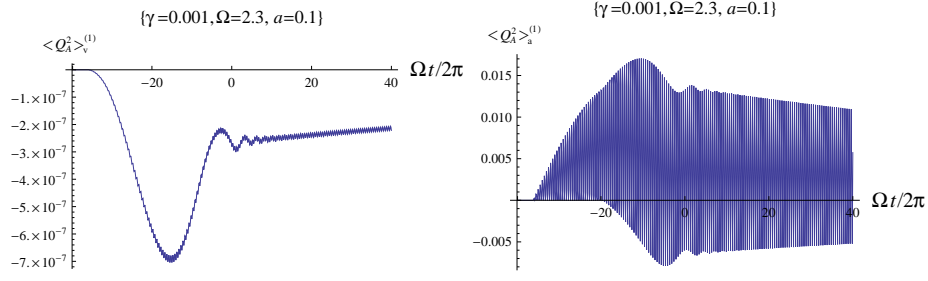


FIG. 6: Numerical results for the first order corrections to $\langle Q_A^2(t) \rangle_v$ (left) and $\langle Q_A^2(t) \rangle_a$ (right) from mutual influences with $d = 10$, $\alpha = 1.4$, and $\beta = 0.2$. One can see the profile of the envelope of the oscillating $\langle Q_A, Q_B \rangle_v$ in Fig. 5.

because of the mode sum $\int d^3k$. Nevertheless, we can express the corrected correlators up to the N -th order mutual influences as, for example,

$$\langle Q_i(\tau_i), Q_j(\tau_j) \rangle_{v,a} \approx \sum_{m=0}^N \sum_{n=0}^N \langle Q_i^{(m)}(\tau_i), Q_j^{(n)}(\tau_j) \rangle_{v,a}, \quad (31)$$

where the (m, n) -th order correlator $\langle Q_i^{(m)}(\tau_i), Q_j^{(n)}(\tau_j) \rangle$ can be obtained recursively from those of lower orders by

$$\langle Q_i^{(m)}(\tau_i), Q_j^{(n)}(\tau_j) \rangle_{v,a} = \frac{2\gamma}{\Omega} \int_{\tau_j^{(0)}}^{\tau_j} d\tilde{\tau} \theta(\tau_j^{ret}(\tilde{\tau}) - \tau_j^{(n-1)}) \frac{K(\tau_j - \tilde{\tau})}{R_{\bar{j} \rightarrow j}(\tilde{\tau})} \langle Q_i^{(m)}(\tau_i), Q_{\bar{j}}^{(n-1)}(\tau_j^{ret}(\tilde{\tau})) \rangle_{v,a} \quad (32)$$

$(m, n \geq 1)$ and their τ_i or τ_j derivatives.

From (29)–(32) we see that the N -th order corrections are roughly $O((\gamma/\Omega d)^N)$ compared with the magnitude of the zeroth order correlators. The presence of the oscillating function $K(\tau - \tilde{\tau})$ in the integrand of (30) further indicates that one detector (j) will be influenced very little by the off-resonant part of $q_{\bar{j}}^{(\mu)(n-1)}(\tau_j^{ret}(\tilde{\tau}))/R_{\bar{j} \rightarrow j}(\tilde{\tau})$ from the other detector (\bar{j}) in the weak coupling limit. In our setup since the trajectories of the two detectors are asymmetric, the retarded field solution from detector j will always be red- or blue-shifted in view of detector \bar{j} . So most of $q_{\bar{j}}^{(\mu)(n-1)}(\tau_j^{ret}(\tilde{\tau}))/R_{\bar{j} \rightarrow j}(\tilde{\tau})$ are off-resonant and thus mutual influences can be very small even though the magnitudes of $q_{\bar{j}}^{(\mu)(n-1)}(\tau_j^{ret}(\tilde{\tau}))/R_{\bar{j} \rightarrow j}(\tilde{\tau})$ appear larger.

According to our analysis and numerical results, mutual influences are indeed negligible in perturbative regime when the distance between the detectors is always large, i.e., $\gamma/\Omega d \ll 1$. For example, our numerical results show that when $\gamma = 10^{-3}$, $\Omega = 2.3$, $a = 0.1$, $d = 10$, $\Lambda_0 = \Lambda_1 = 20$, the magnitudes of the first order corrections $\langle Q_A^2(t) \rangle_v^{(1)} \equiv 2 \langle Q_A^{(0)}(t), Q_A^{(1)}(t) \rangle_v + \langle Q_A^{(1)}(t), Q_A^{(1)}(t) \rangle_v$ are less than 10^{-4} of the magnitude of $\langle Q_A^{(0)}(t), Q_A^{(0)}(t) \rangle_v$ (see Figs. 6 (left) and 8 (left)), while the magnitudes of the first order correction $\langle Q_A^2(t) \rangle_a^{(1)} \equiv 2 \langle Q_A^{(0)}(t), Q_A^{(1)}(t) \rangle_a + \langle Q_A^{(1)}(t), Q_A^{(1)}(t) \rangle_a$ are about 10^{-3} that of $\langle Q_A^{(0)}(t), Q_A^{(0)}(t) \rangle_a$ (see Figs. 6 (right) and 7 (left)). The corrections become even smaller as we decrease γ or increase d . The ratio $\langle Q_A^2(t) \rangle_v^{(1)} / \langle Q_A^2(t) \rangle_v^{(0)}$ is smaller than $\langle Q_A^2(t) \rangle_a^{(1)} / \langle Q_A^2(t) \rangle_a^{(0)}$ simply because the v-part of the zeroth order cross correlator $\langle Q_A(t), Q_B(t) \rangle_v^{(0)}$ is suppressed when d is large (see Eq. (B1)), while $\langle Q_A(t), Q_B(t) \rangle_a^{(0)}$ is independent of d .

D. Entanglement dynamics with weak coupling and large separation

Combining all the above elements with weak coupling and large separation, examples of the evolution of the a-part of the correlators are shown in Fig. 7, while those of the v-part of the self correlators are shown in Fig. 8.

The dynamics of quantum entanglement between the two detectors in Gaussian state can be found straightforwardly by examining the behavior of the quantity Σ [10, 31] and the logarithmic negativity E_N [32] defined by

$$\Sigma \equiv \det \left[\mathbf{V}^{PT} + \frac{i\hbar}{2} \mathbf{M} \right] = \left(c_+^2 - \frac{\hbar^2}{4} \right) \left(c_-^2 - \frac{\hbar^2}{4} \right), \quad (33)$$

$$E_N \equiv \max \{0, -\log_2 2c_-\}, \quad (34)$$

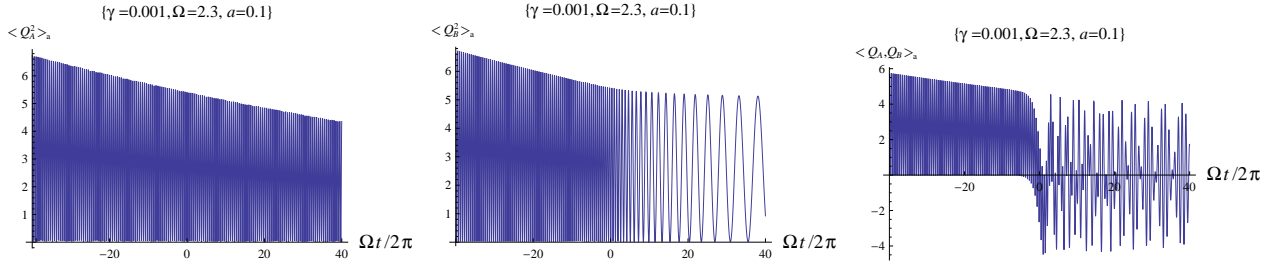


FIG. 7: The evolution of $\langle Q_A^2 \rangle_a$ (left), $\langle Q_B^2 \rangle_a$ (middle), and $\langle Q_A, Q_B \rangle_a$ (right) with $\alpha = 1.4$, $\beta = 0.2$ and $d = 10$ in Minkowski time. The oscillations are consequences of choosing the initial state of the detectors as a squeezed state. Time dilation in the results for detector B is manifest after $at > -0.114$, which makes the cross correlators behave more irregularly.

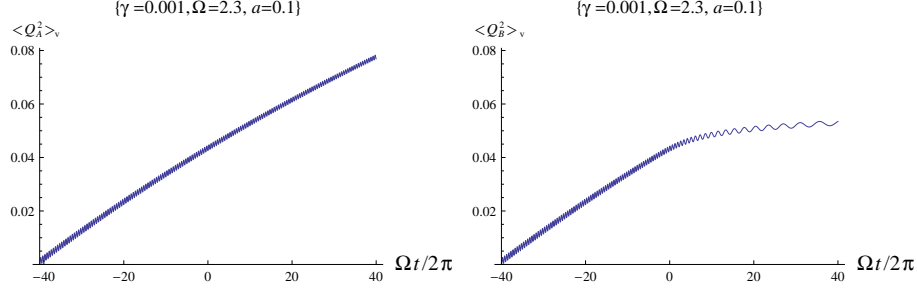


FIG. 8: Evolution of the v-part of the self correlators $\langle Q_A^2 \rangle_v$ and $\langle Q_B^2 \rangle_v$ in Minkowski time with $d = 10$ and $\Lambda_0 = \Lambda_1 = 20$. Again, time dilation in the results for detector B is manifest after $at > -0.114$. The contributions from the differences shown in Fig. 3 are very small and not significant in these plots.

where \mathbf{M} is the symplectic matrix $\mathbf{1} \otimes (-i)\sigma_y$, \mathbf{V}^{PT} is the partial transpose $((Q_A, P_A, Q_B, P_B) \rightarrow (Q_A, P_A, Q_B, -P_B))$ of the covariance matrix \mathbf{V} in (13), and (c_+, c_-) is the symplectic spectrum of $\mathbf{V}^{PT} + (i\hbar/2)\mathbf{M}$, given by

$$c_{\pm} \equiv \left[\frac{Z \pm \sqrt{Z^2 - 4 \det \mathbf{V}}}{2} \right]^{1/2} \quad (35)$$

with $Z \equiv \det \mathbf{v}_{AA} + \det \mathbf{v}_{BB} - 2 \det \mathbf{v}_{AB}$. For the detectors in a Gaussian state, the reduced state of the detectors is entangled if and only if $c_- < \hbar/2$ [31], when $E_{\mathcal{N}} > 0$ and $\Sigma < 0$. The value of $E_{\mathcal{N}}$ indicates the degree of entanglement: we say the two detectors have a stronger entanglement if the associated $E_{\mathcal{N}}$ is greater. However it is more convenient to use Σ in calculating the disentanglement time [9, 10].

An example of the sudden death of entanglement is given in Fig. 9, where we see that the curves with $a \neq 0$ are stretched horizontally after $t \approx 0$ due to the time dilation of the moving detector B . This increases the disentanglement time.

The contribution by the v-part of the cross correlators to entanglement dynamics is suppressed efficiently when the coupling is weak (here $\gamma = 0.001$, not quite weak, though) and the distance is large (here $d = 10$). In the difference $E_{\mathcal{N}} - (E_{\mathcal{N}}|_{\langle \mathcal{R}_A(t), \mathcal{R}_B(\tau(t)) \rangle_v = 0})$ shown in Fig. 9 (middle), we recognize the profile of the envelopes of the oscillating cross correlators in Fig. 5. Thus the nonvanishing cross correlators tend to enhance the degree of entanglement between the detectors. However the enhancement of $E_{\mathcal{N}}$ is tiny — so tiny that it is safe to neglect the v-part of the cross correlators and skip the time-consuming computation for them in the weak-coupling limit with long initial distances and large initial entanglement between the detectors.

In contrast, while the value of each v-part of the self correlators is small compared with its a-counterpart, they are crucial in obtaining the entanglement dynamics. If one sets all the v-parts of the self correlators to zero, the evolution of Σ and the logarithmic negativity $E_{\mathcal{N}}$ will be very different (for example, see [10].) Therefore in the perturbative regime with large initial distance and entanglement between the detectors, the zeroth order of the a-part of all correlators as well as the v-part of the self correlators are enough to give the entanglement dynamics to high accuracy.

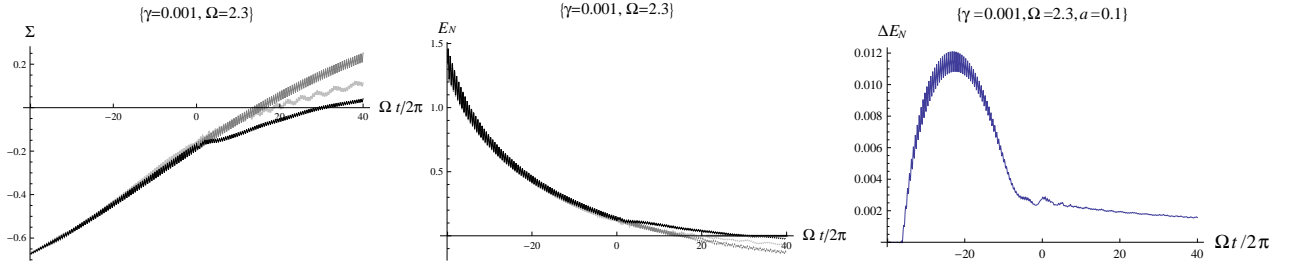


FIG. 9: Numerical results with $\alpha = 1.4$, $\beta = 0.2$ in (12) for the quantity $\Sigma(t)$ (left) the logarithmic negativity $E_N(t)$ (middle, solid curves), both indicating the degree of entanglement between the detector at (3) with $d = 10$ and the detector going along (4). The gray, the thick-lightgray, and the black curves in both plots represent the results with $a = 0, 0.1$, and 2 , respectively, where the $a = 0$ case corresponds to those for two inertial detectors both at rest in space and separated at a distance $d = 10$ in the same initial state [9]. Quantum entanglement experiences sudden death at $(\Omega t_{dE}/2\pi) \approx 16$ for $a = 0.1$ and ≈ 30 for $a = 2$ when E_N touches 0 and Σ crosses 0. One can see that the larger the value of a , the longer the disentanglement time t_{dE} , due to the time dilation of the moving detector B in this setup. (Right) The difference $\Delta E_N \equiv E_N - (E_N|_{\langle \mathcal{R}_A(t), \mathcal{R}'_B(\tau(t)) \rangle_v=0})$ for $a = 0.1$. One can see the profile of the envelopes of the oscillating cross correlators in Fig. 5. The value of the difference is tiny compared with the value of E_N (the largest ratio is about 3% around $t \approx -18(2\pi)/\Omega$).

IV. SUMMARY

We have demonstrated that the dynamics of a UD detector in non-uniform acceleration are similar to those of a harmonic oscillator in contact with a “thermal” bath at a time-varying “temperature” in the weak coupling regime, while non-adiabatic changes of proper acceleration will create oscillations on top of the smoothly evolving values of the correlators. The behavior of the detector is determined by the kinematics in its history rather than by assuming the presence of a horizon that does not exist until late time.

In our model with weak coupling to the field, large spatial separation and large initial entanglement between the detectors, the higher-order corrections from mutual influences are negligible and the early-time behavior of the detectors are dominated by the zeroth order of the a-parts of the self and cross correlators of the detectors, which correspond to the initial state of the detectors. The zeroth order contribution of the v-parts of the *self* correlators of the detectors, which corresponds to the response of the detectors to the field, is also crucial for entanglement dynamics, though their values are small compared to their a-counterparts. While the zeroth order of the v-part of the *cross* correlators would in general enhance quantum entanglement between the detectors, their values are even smaller than others and negligible in the perturbative regime if the initial degree of entanglement between the detectors is large.

We have chosen a trajectory for detector B such that it is approximately at rest when its proper time τ is negatively large, and almost uniformly accelerated when τ is positively large. As expected, the entanglement dynamics of the detectors here are similar to those in the case of two inertial detectors [9] when τ is negatively large, and look like those in the case with one inertial detector and one uniformly accelerated detector when τ is positively large [10]. These results are commensurate with those obtained previously using alternative methods for evaluating entanglement dynamics of detectors in relative non-uniform acceleration [27]. While the dynamics of the correlators are more subtle during the transition of detector B from zero to finite accelerations, such interesting behavior is negligible in computing the entanglement dynamics in the perturbative regime. In our model we do see sudden death of entanglement (see Fig. 9). As noted earlier in [10], however, the acceleration in this case increases rather than decreases the disentanglement time because of the time dilation of the moving detector B observed in the conventional Minkowski coordinate, though a higher Unruh temperature is experienced by detector B at late times.

A number of interesting directions for further research emerge based on our results. A time-reversed setup where detector B begins in the distant past as almost uniformly accelerated then becomes approximately inertial in the distant future could be considered. Combining these results with those obtained in this paper, the case with the world lines of the detectors similar to the ones in the twin paradox [12] becomes straightforward in weak coupling limit with large spatial separation [28]. Extending our work to cosmological settings that go beyond idealizations previously considered [33] is another avenue for further research. Wider parameter ranges, such as those beyond weak coupling, small acceleration and/or large spatial separation regimes are also worth studying.

Acknowledgement BLH and SYL wish to thank the hospitality of the Perimeter Institute for hosting their visits in Spring 2008 where this joint work began. This work is supported in part by the Natural Sciences and Engineering Research Council of Canada, the Nation Science Council of Taiwan under the Grant No. NSC 99-2112-M-018-001-

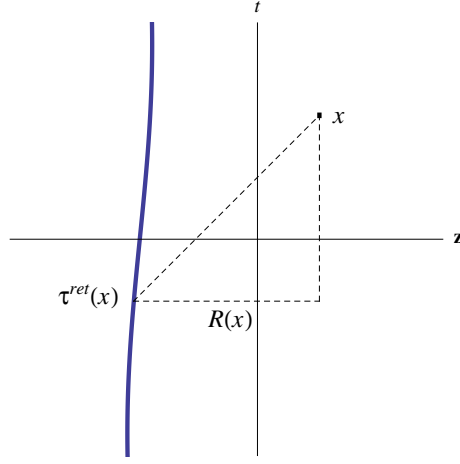


FIG. 10: Definitions of $\tau^{ret}(x)$ and $R(x)$. The thick curve is the world line of a detector parametrized by its proper time τ .

MY3, and the NSF Grant No. PHY-0801368.

Appendix A: Retarded distance and retarded time

For a massless field in (3+1)D flat spacetime, the retarded time $\tau^{ret}(x^\mu)$ associated with a field observed at the spacetime point x^μ is defined as the proper time τ of the field source at which the trajectory of the point-like source $z^\mu(\tau)$ intercepts the past light cone of x^μ . It is given by the solution to $\sigma(x^\mu, z^\mu(\tau^{ret})) = 0$ where

$$\sigma(x^\mu, z^\mu(\tau)) = -\frac{1}{2} (x^\mu - z^\mu(\tau)) (x_\mu - z_\mu(\tau)) \quad (\text{A1})$$

is Synge's world function. Since σ is quadratic, when $\sigma = 0$ is satisfied, the Dirac delta function $\delta(\sigma)$ in the retarded Green's function of the field will give an $1/R$ factor in τ -integrals involving it, where

$$R = \left| \frac{d\sigma}{d\tau} \right|_{\sigma=0} \quad (\text{A2})$$

is a function of x^μ and the location of the source at the retarded time $\tau^{ret}(x^\mu)$. We call R the retarded distance (see Fig. 10).

For detector A , one has

$$\sigma = -\frac{1}{2} [D(\mathbf{x})^2 - (t - x^0)^2], \quad (\text{A3})$$

where $D(\mathbf{x}) \equiv \sqrt{(x^1 + d)^2 + \rho^2}$ and $\rho^2 \equiv x_2^2 + x_3^2$. Solving $\sigma = 0$, the retarded time of detector A is found to be

$$\tau_A^{ret}(x) = t^{ret}(x) \equiv x^0 - D(\mathbf{x}). \quad (\text{A4})$$

So the retarded distance is $R = D(\mathbf{x})$. In particular, at the position of the detector B , the retarded distance from A to B is

$$R_{A \rightarrow B}(\tau) = D(z_B^\mu(\tau)). \quad (\text{A5})$$

For detector B , one has

$$\sigma = -\frac{1}{2} \left[\rho^2 - UV + \frac{1}{a^2} + \frac{U}{a} e^{a\xi} - \frac{2x^0}{a} e^{-a\xi} - \frac{e^{-2a\xi}}{a^2} \right], \quad (\text{A6})$$

where $U \equiv x^0 - x^1$ and $V \equiv x^0 + x^1$. So the retarded time of the field sourced from detector B and observed by detector A at $(t, -d, 0, 0)$ is $\tau_B^{ret} = \tau(\xi^{ret}(t))$, where

$$\xi^{ret}(t) = \frac{1}{a} \sinh^{-1} \left[\frac{a}{2} (t - d) \right], \quad (\text{A7})$$

and the retarded distance from detector B to A is

$$R_{B \rightarrow A}(t) = \left| \frac{1}{2\ell\sqrt{\ell^2 + 1}} \left[\frac{2}{a}\ell^3 + 2t\ell^2 + t + d \right] \right|, \quad (\text{A8})$$

where $\ell \equiv [a(d - t) + \sqrt{4 + a^2(d - t)^2}]/2$.

Appendix B: Remarks on numerical calculation for correlators

1. Self Correlators

The periodicity of the integrand of (20) can help to reduce the computation time. For example, from (20) one has

$$\begin{aligned} \delta \langle Q_B^2(\tau + (2\pi/\Omega)) \rangle_v &= \frac{2\gamma\hbar}{\pi m_0 \Omega^2} \int_{\tau_0}^{\tau + (2\pi/\Omega)} d\tilde{\tau} d\tilde{\tau}' K(\tau + (2\pi/\Omega) - \tilde{\tau}) K(\tau + (2\pi/\Omega) - \tilde{\tau}') \tilde{f}(\tilde{\tau}, \tilde{\tau}') \\ &= \frac{2\gamma\hbar}{\pi m_0 \Omega^2} e^{-4\pi\gamma/\Omega} \left[\int_{\tau_0}^{\tau} d\tilde{\tau} + \int_{\tau}^{\tau + (2\pi/\Omega)} d\tilde{\tau} \right] \left[\int_{\tau_0}^{\tau} d\tilde{\tau}' + \int_{\tau}^{\tau + (2\pi/\Omega)} d\tilde{\tau}' \right] K(\tau - \tilde{\tau}) K(\tau - \tilde{\tau}') \tilde{f}(\tilde{\tau}, \tilde{\tau}') \\ &= e^{-4\pi\gamma/\Omega} \delta \langle Q_B^2(\tau) \rangle_v + \frac{2\gamma\hbar}{\pi m_0 \Omega^2} e^{-4\pi\gamma/\Omega} \times \\ &\quad \left[\int_{\tau_0}^{\tau} d\tilde{\tau} \int_{\tau}^{\tau + (2\pi/\Omega)} d\tilde{\tau}' + \int_{\tau}^{\tau + (2\pi/\Omega)} d\tilde{\tau} \int_{\tau_0}^{\tau} d\tilde{\tau}' + \int_{\tau}^{\tau + (2\pi/\Omega)} d\tilde{\tau} \int_{\tau}^{\tau + (2\pi/\Omega)} d\tilde{\tau}' \right] K(\tau - \tilde{\tau}) K(\tau - \tilde{\tau}') \tilde{f}(\tilde{\tau}, \tilde{\tau}'). \end{aligned}$$

Thus one can obtain $\delta \langle Q_B^2(\tau + (2\pi/\Omega)) \rangle_v$ by adding the previously obtained $\delta \langle Q_B^2(\tau) \rangle_v$ multiplied by a factor $e^{-4\pi\gamma/\Omega}$ to the result of an integration over an L-shaped strip with width $2\pi/\Omega$ and total length $2\tau + 2\pi/\Omega$, rather than a large $[\tau + (2\pi/\Omega)] \times [\tau + (2\pi/\Omega)]$ square, in the $\tilde{\tau}\tilde{\tau}'$ -plane. By designing the grid such that there are exactly $N \in \mathbb{N}$ lattice sites in a natural period of detector $2\pi/\Omega$ in $\tilde{\tau}$ or $\tilde{\tau}'$, one can improve the computation time for evaluating $\delta \langle Q_B^2(\tau) \rangle_v$ numerically in duration $\tau_f - \tau_0$ from $O[(\tau_f - \tau_0)^3]$ to $O[(\tau_f - \tau_0)^2]$ [39].

2. Cross Correlators

In (28) the non-linear t -dependence of $\tau(t)$ is manifest after $t \gtrsim 0$, then the domain $(\tau(t_0), \tau(t))$ that $\tilde{\tau}'$ is integrated over will not increase in equal time-intervals for each step in t . So the trick of periodicity in obtaining $\delta \langle Q_B^2 \rangle_v^{(0)}$ cannot be applied. However we can still calculate $\langle Q_A(t), Q_B(\tau') \rangle_v^{(0)}$ over the $t\tau'$ -plane, where the periodicity of the integrand can be employed, and then extract $\langle Q_A(t), Q_B(\tau(t)) \rangle_v^{(0)}$ by letting $\tau' = \tau(t)$ and interpolating. The results of $\langle Q_A(t), Q_B(\tau') \rangle_v^{(0)}$ here is also useful in calculating the mutual influences in Section III C.

The integrand of (28) appears to be singular at $\tilde{\tau} = d + a^{-1}e^{-a\tilde{\xi}'}$ and $\tilde{\tau} = d + 2a^{-1}\cosh a\tilde{\xi}'$ if $\epsilon = 0$. However the presence of the nonzero ϵ and the fact that the denominators in the square bracket of the above expression are linear in $\tilde{\tau}$ makes it possible to deal with the “singularities” in the following way:

$$\begin{aligned} &\langle Q_A(t), Q_B(\tau(t)) \rangle_v^{(0)} \\ &= \frac{2\gamma\hbar}{\pi m_0 \Omega^2} \text{Re} \int_{\tau(t_0)}^{\tau(t)} d\tilde{\tau}' \int_{t_0}^t d\tilde{\tau} \frac{K(\tau(t) - \tilde{\tau}')}{2d + a^{-1}e^{a\tilde{\xi}'}} \left[\frac{K(t - \tilde{\tau}) - K(t + d + a^{-1}e^{-a\tilde{\xi}'}) + K(t + d + a^{-1}e^{-a\tilde{\xi}'})}{\tilde{\tau} + d + a^{-1}e^{-a\tilde{\xi}'} - i\epsilon} \right. \\ &\quad \left. - \frac{K(t - \tilde{\tau}) - K(t - d - 2a^{-1}\cosh a\tilde{\xi}') + K(t - d - 2a^{-1}\cosh a\tilde{\xi}')}{\tilde{\tau} - d - 2a^{-1}\cosh a\tilde{\xi}' - i\epsilon} \right], \\ &= \frac{2\gamma\hbar}{\pi m_0 \Omega^2} \text{Re} \int_{\tau(t_0)}^{\tau(t)} d\tilde{\tau}' \times \\ &\quad \left\{ \int_{t_0}^t d\tilde{\tau} \frac{K(\tau(t) - \tilde{\tau}')}{2d + a^{-1}e^{a\tilde{\xi}'}} \left[\frac{K(t - \tilde{\tau}) - K(t + d + a^{-1}e^{-a\tilde{\xi}'})}{\tilde{\tau} + d + a^{-1}e^{-a\tilde{\xi}'}} - \frac{K(t - \tilde{\tau}) - K(t - d - 2a^{-1}\cosh a\tilde{\xi}')}{\tilde{\tau} - d - 2a^{-1}\cosh a\tilde{\xi}'} \right] \right\} \end{aligned}$$

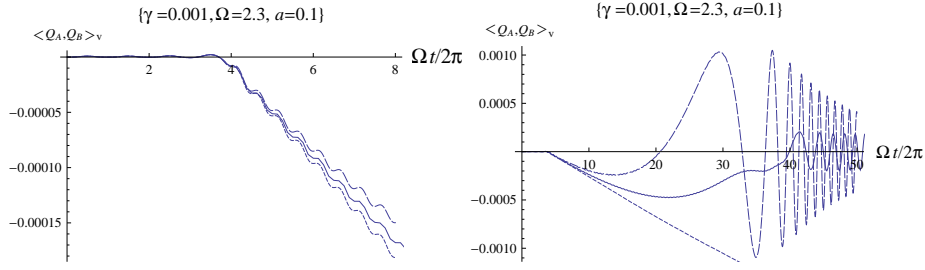


FIG. 11: Early-time evolution of the cross correlator $\langle Q_A(t), Q_B(\tau(t)) \rangle_v$ with $d = 10$ (solid curves) shown in Fig. 5 compared with the analytical results of the cases with two inertial detectors sitting at a fixed distance in Ref. [9]. The left plot is a close up of the very early-time behavior in the right plot. The dotted curves are obtained by inserting the initial distance $d + (t_0 + \sqrt{t_0^2 + (2/a^2)})$ between the two detectors, which is temporally constant, into the fixed-distance analytical expressions in [9], while the dashed curves are obtained by naively inserting the distance $d + (t + \sqrt{t^2 + (2/a^2)})$ at each moment t into the same fixed-distance analytic expression. One can see that at very early times the value of the numerical result here agrees with the analytic results quite well.

$$+K \left(t + d + a^{-1}e^{-a\tilde{\xi}'} \right) \ln \left| \frac{t + d + a^{-1}e^{-a\tilde{\xi}'}}{t_0 + d + a^{-1}e^{-a\tilde{\xi}'}} \right| - K \left(t - d - 2a^{-1} \cosh a\tilde{\xi}' \right) \ln \left| \frac{t - d - 2a^{-1} \cosh a\tilde{\xi}'}{t_0 - d - 2a^{-1} \cosh a\tilde{\xi}'} \right| \Bigg\}. \quad (\text{B1})$$

Those terms in the square bracket of the last expression are smooth, so we can apply elementary numerical methods such as Simpson's rule to carry out the 2D integration to high accuracy. The remainder is a one-dimensional integral over $\tilde{\tau}'$, which is easy to deal with. Although the integrand of the latter appears to have a logarithmic singularity at $t_0 + d + a^{-1}e^{-a\tilde{\xi}'} = 0$, the integral is still finite (and well defined by ϵ). Note that $|t_0 - d - 2a^{-1} \cosh a\tilde{\xi}'|$ is always positive here, and the combination $K(x) \ln |x|$ is regular at $|t - d - 2a^{-1} \cosh a\tilde{\xi}'| = 0$ and $|t + d + a^{-1}e^{-a\tilde{\xi}'}| = 0$.

Comparing the numerical results for the cross correlator $\langle Q_A(t), Q_B(\tau(t)) \rangle_v^{(0)}$ and the analytical results for the case of two inertial detectors sitting at fixed distance [9] in Fig. 11, we find excellent agreement at very early times when the distance between the two detectors is almost constant.

Appendix C: Behavior of $\delta \langle Q_B^2 \rangle_v$ during and after transition

The jump of $\delta \langle Q_B^2 \rangle_v$ in Fig. 2 is actually a smooth increase at the same rate as the square of the proper acceleration (11) grows. The behavior of $\delta \langle Q_B^2 \rangle_v$ and the approximately universal value of the height of the jump divided by a^2 in Fig. 2 can be estimated as follows.

The contour plot of f defined in (27) on the $\chi\chi'$ -plane is shown in Fig. 12. One can see that when both $\chi, \chi' \lesssim -1$, the value of f is very small, and when $\chi, \chi' \gtrsim 0$, a ridge emerges along $\chi = \chi'$. During the transition $-1 \lesssim (\chi, \chi') \lesssim 2$, the values of f in the domain of integration are roughly independent of $\Delta \equiv \chi - \chi'$ so all the contours are almost perpendicular to the $X \equiv (\chi + \chi')/2$ directions. Expanding f in Δ about $\Delta = 0$ yields

$$f(\chi, \chi') = f^{(0)}(X) - \frac{(1 - 4e^{-2X})}{240(1 + e^{-2X})^4} \Delta^2 + O(\Delta^4). \quad (\text{C1})$$

where

$$f^{(0)}(X) \equiv \frac{1}{12(1 + e^{-2X})^2}. \quad (\text{C2})$$

While the zeroth order term of the above expansion $f^{(0)}(X)$ undergoes significant change around $-1 \lesssim X \lesssim 2$ (see Fig. 13 (Left)), the error of the approximation $f(X, \Delta) \approx f^{(0)}(X)$ is always less than 0.05 times of the value of $f(X, \Delta)$ in the region $-1 \leq X \leq 2$ and $X - 2 \leq \Delta \leq 2 - X$.

During the transition $-1 \leq X \leq 2$, the integral in (26) is mainly contributed by the integrand in $0 \leq X \leq 2$, where $a(\tau - \tau(\xi)) \approx a\xi(\tau) - \chi$ according to (8). So we further approximate

$$K(\tau - \tau(\chi/a)) \approx e^{-\gamma(a\xi(\tau) - \chi)/a} \sin \frac{\Omega}{a} (a\xi(\tau) - \chi). \quad (\text{C3})$$

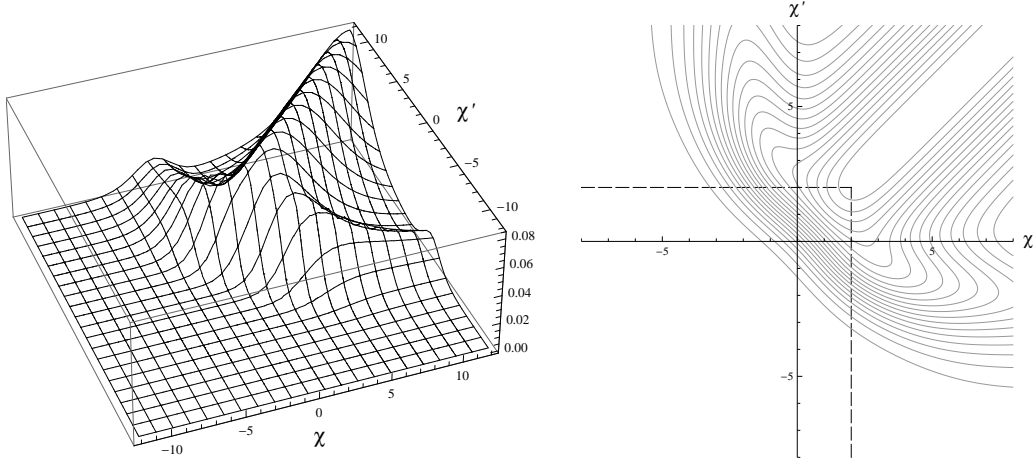


FIG. 12: The topography (left) and the contour plot (right) of $f(\chi, \chi')$ defined in (27).

The error from the deviation of the linearization $a\xi(\tau) - \chi$ from $a(\tau - \tau(\xi))$ for $X < 0$ will be suppressed efficiently because f is small while $K(\tau, \tau(\chi/a))$ oscillates wildly there.

Let $X_2(\tau) \equiv a\xi(\tau)$. Combining the above approximations for $f \approx f^{(0)}$ in (C2) and K in (C3), and neglecting the contribution from the $X < -1$ region, we have

$$\begin{aligned} \delta \langle Q_B^2(\tau) \rangle_v &\approx \frac{2\gamma\hbar}{\pi m_0 \Omega^2} \int_{\chi(\tau_0)}^{X_2} dX \int_{2(X_2-X)}^{-2(X_2-X)} \frac{d\Delta}{2} \left[\cos \frac{\Omega}{a} \Delta - \cos \frac{2\Omega}{a} (X_2 - X) \right] \frac{e^{-2\gamma(X_2-X)/a}}{12(1 + e^{-2X})^2} \\ &= \frac{\gamma\hbar}{12\pi m_0 \Omega^2} \frac{2a}{\Omega} \left(1 - \Omega \frac{\partial}{\partial \Omega} \right) \text{Re} \int_{\chi(\tau_0)}^{X_2} dX \frac{e^{-2(\gamma-i\Omega)(X_2-X)/a}}{i(1 + e^{-2X})^2}, \end{aligned} \quad (\text{C4})$$

which is expected to be a good approximation for $0 \lesssim X_2 \lesssim 2$ if $\chi(\tau_0) \ll -1$. The above integral has an analytic result in a closed form, which is a function of X_2 . For $X_2 \geq 2$ and $\chi(\tau_0)$ is negatively large, most of the terms goes to zero except the following:

$$\delta \langle Q_B^2(\tau) \rangle_v \approx \frac{\gamma\hbar a}{12\pi m_0 \Omega^3} \left(1 - \Omega \frac{\partial}{\partial \Omega} \right) \text{Re} \left[\frac{(1 + \mathcal{W})}{i(2 + \mathcal{W})} e^{4X_2} {}_2F_1(1, 2 + \mathcal{W}, 3 + \mathcal{W}, -e^{2X_2}) \right], \quad (\text{C5})$$

where $\mathcal{W} \equiv (\gamma + i\Omega)/a$, and ${}_2F_1$ is the hypergeometric function, which oscillates in X_2 around a finite, nonzero constant for $X_2 \geq 2$, whose value can be obtained by, mathematically, taking $X_2 \rightarrow \infty$ when the oscillation is damped out (see Fig. 13 (Right)). So we end up with

$$\begin{aligned} \delta \langle Q_B^2(\tau) \rangle_v|_{a\xi(\tau)=X_2=2} &\approx \frac{\gamma\hbar a}{12\pi m_0 \Omega^3} \left(1 - \Omega \frac{\partial}{\partial \Omega} \right) \text{Re} \left[-ie^{2X_2} + \frac{i(1 + \mathcal{W})}{\mathcal{W}} + O(e^{-2X_2}) \right]_{X_2 \rightarrow \infty} \\ &= \frac{\gamma\hbar a}{12\pi m_0 \Omega^3} \left(1 - \Omega \frac{\partial}{\partial \Omega} \right) \frac{a\Omega}{(\gamma^2 + \Omega^2)} \\ &= \frac{\gamma\hbar a^2}{6\pi m_0 (\gamma^2 + \Omega^2)^2}, \end{aligned} \quad (\text{C6})$$

which is consistent with our observations in Fig. 2 and Eq. (22).

Now the numerical behavior of $\delta \langle Q_B^2(\tau) \rangle_v$ can be understood as follows. The domain of the $\chi\chi'$ -integration is the square with both $\chi, \chi' \in [a\xi(\tau_0), a\xi(\tau)]$. $X_2(\tau) \equiv a\xi(\tau)$ increases as τ increases. When the vertex $(X_2(\tau), X_2(\tau))$ of the domain touches $X \approx -1$, the growth of $f(\chi, \chi')$ becomes significant so $\delta \langle Q_B^2(\tau) \rangle_v$ starts to grow. The latter keeps growing smoothly until the vertex of the domain reaches $X \approx 2$ (the boundary of the domain at this moment is indicated by the dashed lines in Fig. 12 (Right)), then the evolution enters another phase where $\delta \langle Q_B^2(\tau) \rangle_v$ grows slowly in a time scale of $1/2\gamma$ as shown in (25), with oscillations on top of the growing, towards the late-time value $\delta \langle Q_B^2(\infty) \rangle_v$.

To obtain more insight into the behavior of $\delta \langle Q_B^2(\tau) \rangle_v$ after $X_2 \approx 2$, let us consider the following simple approximations. Let $\tau_2 \equiv \tau(\xi)|_{a\xi=2}$. In the region $\tau_2 \leq \tilde{\tau} \leq \tau$ or $\tau_2 \leq \tilde{\tau}' \leq \tau$ we observed that

$$\tilde{f}(\tilde{\tau}, \tilde{\tau}') \approx \tilde{f}^{(0)}(\tilde{\Delta}) \equiv \frac{1}{\tilde{\Delta}^2} - \frac{a^2}{4 \sinh^2(a\tilde{\Delta}/2)} \quad (\text{C7})$$

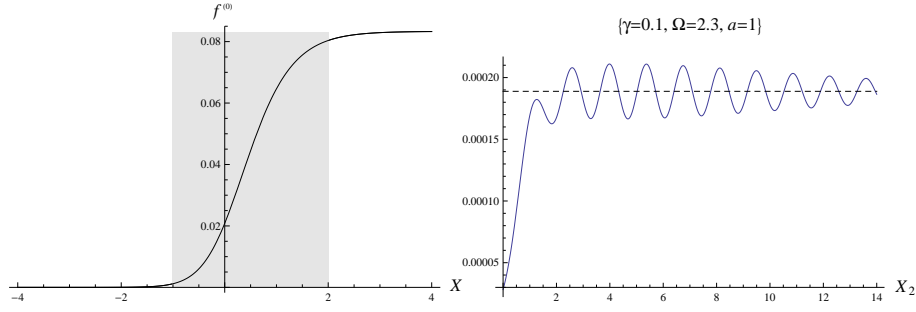


FIG. 13: (Left) The evolution of the zeroth order term of (C1) in X . The value of $f^{(0)}$ changes significantly around $-1 \lesssim X \lesssim 2$ (shaded interval). (Right) The values of the right hand side of Eq. (C5) as a function of X_2 . We see that $\delta \langle Q_B^2(\tau) \rangle_v|_{a\xi(\tau)=X_2}$ grows smoothly from zero after $X_2 \approx 0$, then starts to oscillate about the limiting value of the function as $X_2 \rightarrow \infty$.

in the integrand of (20) with $\tilde{\Delta} \equiv \tilde{\tau}' - \tilde{\tau}$. So $\delta \langle Q_B^2(\tau) \rangle_v$ for $\tau > \tau_2 \gg \tau_0$ can be approximated by

$$\delta \langle Q_B^2(\tau) \rangle_v \approx \delta \langle Q_B^2(\tau) \rangle_v^{(0)} \equiv \frac{2\gamma\hbar}{\pi m_0 \Omega^2} [I_1(\tau) + I_2(\tau)], \quad (\text{C8})$$

where

$$\begin{aligned} I_1 &\equiv \int_{\chi(\tau_0)}^2 d\chi \int_{\chi(\tau_0)}^2 d\chi' K(\tau - \tau(\chi/a)) K(\tau - \tau(\chi'/a)) f^{(0)}(X), \\ I_2 &\equiv \left(\int_{\tau_0}^{\tau} d\tilde{\tau} \int_{\tau_0}^{\tau} d\tilde{\tau}' - \int_{\tau_0}^{\tau_2} d\tilde{\tau} \int_{\tau_0}^{\tau_2} d\tilde{\tau}' \right) K(\tau - \tilde{\tau}) K(\tau - \tilde{\tau}') \tilde{f}^{(0)}(\tilde{\Delta}). \end{aligned} \quad (\text{C9})$$

By modifying the earlier calculation in obtaining (C5), it is straightforward to see

$$I_1 \approx \frac{e^{-2\gamma\eta+4\times 2}}{24\Omega} \text{Re} \left\{ \left(1 - e^{-2i\Omega\eta} \Omega \frac{\partial}{\partial \Omega} \right) \left[\frac{a}{i} \left(\frac{1+\mathcal{W}}{2+\mathcal{W}} \right) {}_2F_1(1, 2+\mathcal{W}, 3+\mathcal{W}, -e^{2\times 2}) \right] \right\} \quad (\text{C10})$$

with $\eta \equiv \tau - \tau_2$ since $\tau \sim \xi (= \chi/a)$ in this region by (8). For I_2 , by noting that the first and the second terms of $\tilde{f}^{(0)}$ in (C7) are nothing but the Hadamard functions of the massless scalar field experienced by an inertial detector and a uniformly accelerated detector with proper acceleration a , respectively [29, 30], we apply the techniques similar to those in Refs. [29] and [23] to obtain

$$\begin{aligned} I_2 &= \frac{\pi m_0 \Omega^2}{2\gamma\hbar} \left[\langle Q^2(\eta_0) \rangle_v|_{a_\mu a^\mu = a^2} - \langle Q^2(\eta_0) \rangle_v|_{a_\mu a^\mu \rightarrow 0} \right] - \\ &\quad \frac{1}{2} \text{Re} \left\{ e^{-2\gamma\eta} \left(1 - e^{-2i\Omega\eta} + \frac{i\Omega}{\gamma} \right) \left[\Gamma(0, \mathcal{W}a\bar{\eta}) - \frac{e^{-(1+\mathcal{W})a\bar{\eta}}}{1+\mathcal{W}} F_{\mathcal{W}}(e^{-a\bar{\eta}}) - \psi(1+\mathcal{W}) + \frac{1}{2\mathcal{W}} + \ln \mathcal{W} \right] + \right. \\ &\quad \left. e^{-2\gamma\eta_0} \left(1 - e^{-2i\Omega\eta_0} + \frac{i\Omega}{\gamma} \right) \left[\Gamma(0, -\mathcal{W}a\bar{\eta}) - \frac{e^{-(1-\mathcal{W})a\bar{\eta}}}{1-\mathcal{W}} F_{-\mathcal{W}}(e^{-a\bar{\eta}}) - \psi(1-\mathcal{W}) - \frac{1}{2\mathcal{W}} + \ln(-\mathcal{W}) \right] \right\} \quad (\text{C11}) \end{aligned}$$

with $\eta_0 \equiv \tau - \tau_0$, $\bar{\eta} \equiv \tau_2 - \tau_0$, $F_y(x) \equiv {}_2F_1(1+y, 1, 2+y, x)$, and the v-part of the self correlator $\langle Q^2(\tau - \tau_0) \rangle_v|_{a_\mu a^\mu = a^2}$ of a uniformly accelerated detector with proper acceleration a moving in a massless scalar field initially in vacuum state (see Eqs. (A3) and (A9) in [23]). In Fig. 14 we illustrate that the above approximation can indeed describe the behavior after $\tau > \tau_2$ qualitatively. The major difference is the amplitude of the non-adiabatic oscillations on top of the rising curve. Since the $1/\tilde{\Delta}^2$ term in \tilde{f} or $\tilde{f}^{(0)}$ in (C7) dominates whenever $|\tilde{\Delta}|$ is large, the error of the above approximation will be localized in the vicinity of $(\tilde{\tau} \approx \tau_2, \tilde{\tau}' < \tau_2)$ and $(\tilde{\tau} < \tau_2, \tilde{\tau}' \approx \tau_2)$ with small $\tilde{\tau} - \tilde{\tau}'$. As shown in Fig. 15 (right), $\tilde{f}^{(0)} - \tilde{f}$ is mostly positive, so the approximation (C8) usually gives the non-adiabatic oscillations a larger amplitude than the true amplitude, while these oscillations will be damped out at late times. In the weak coupling limit, the approximation (C8) behaves similarly to (25).

The behavior of $\delta \langle Q_B, P_B \rangle_v$ during the transition can be obtained straightforwardly since $\langle Q_B(\tau), P_B(\tau) \rangle_v = \partial_\tau \langle Q_B^2(\tau) \rangle_v / 2$. For $\delta \langle P_B^2 \rangle$, the calculation is similar except that the functions $K(\tau - \tau(\chi/a))$ in (26) are replaced by

$$\begin{aligned} K'(\tau - \tau(\chi/a)) &= e^{-\gamma(\tau - \tau(\chi/a))} [\Omega \cos \Omega(\tau - \tau(\chi/a)) - \gamma \sin \Omega(\tau - \tau(\chi/a))] \\ &\approx e^{-\gamma(a\xi(\tau) - \chi)/a} \left[\Omega \cos \frac{\Omega}{a} (a\xi(\tau) - \chi) - \gamma \sin \frac{\Omega}{a} (a\xi(\tau) - \chi) \right] \end{aligned} \quad (\text{C12})$$

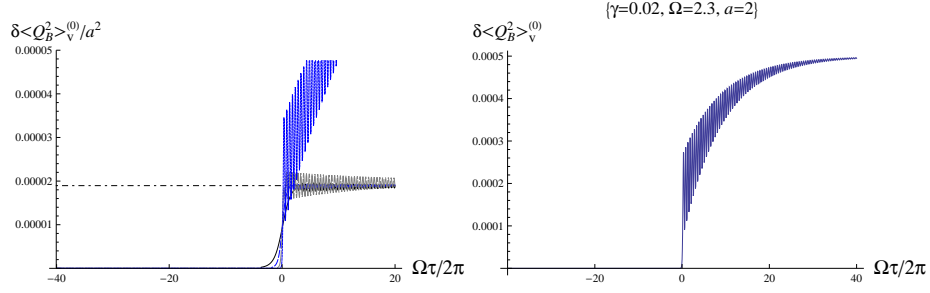


FIG. 14: Approximated evolution of $\delta \langle Q_B^2(\tau) \rangle_v$ by (C8). The left and the right plots are made for comparison with the lower-left plot of Figure 2 and the left plot of Figure 4. Our approximation agrees well with the numerical results qualitatively, except the non-adiabatic oscillations are over-estimated. The horizontal dot-dashed line in the left plot indicates the value of Q/a^2 with Q defined in (22).

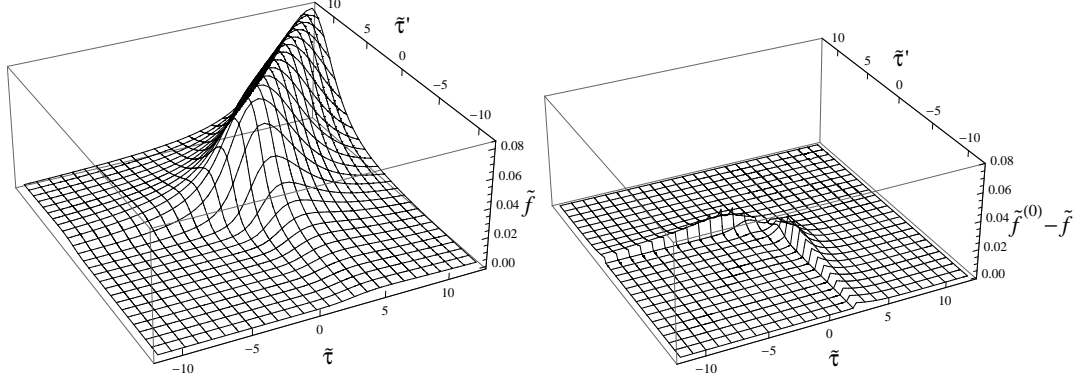


FIG. 15: A comparison between \tilde{f} given in (21) (left) and the error of our approximation $\tilde{f}^{(0)} - \tilde{f}$ (right) on the $\tilde{\tau}\tilde{\tau}'$ -plane. Here $a = 1$, $\tilde{f}^{(0)} = f^{(0)}(X(\tilde{\tau}, \tilde{\tau}'))$ defined in (C2) for $\tilde{\tau}, \tilde{\tau}' < \tau_2$, and $\tilde{f}^{(0)}(\tilde{\tau}, \tilde{\tau}')$ defined in (C7) otherwise. One can see that the error is quite localized and mostly positive.

during $-1 \lesssim X \lesssim 2$. This gives $\delta \langle P_B^2(\tau) \rangle_v|_{a\xi(\tau)=X_2} \approx 0$ as $X_2 \rightarrow \infty$, which is consistent with the observations in Figs. 3 and 4 that there is no significant jump for $\delta \langle P_B^2(\tau) \rangle_v$ around $\tau \approx 0$.

-
- [1] W. G. Unruh, Phys. Rev. D **14**, 870 (1976).
 - [2] <http://isrqi.org>
 - [3] P. M. Alsing and G. J. Milburn, Phys. Rev. Lett. **91**, 180404 (2003).
 - [4] R. Schützhold and W. G. Unruh, preprint [quant-ph/0506028].
 - [5] I. Fuentes-Schuller and R. B. Mann, Phys. Rev. Lett. **95**, 120404 (2005).
 - [6] P. M. Alsing, I. Fuentes-Schuller, R. B. Mann, and T. E. Tessier Phys. Rev. A **74**, 032326 (2006).
 - [7] D. C. M. Ostapchuk, *Entanglement in Non-inertial Frames*, Master thesis (University of Waterloo, 2008).
 - [8] D. C. M. Ostapchuk and R. B. Mann, Phys. Rev. A **79**, 042333 (2009).
 - [9] S.-Y. Lin and B. L. Hu, Phys. Rev. D **79**, 085020 (2009).
 - [10] S.-Y. Lin, C.-H. Chou, and B. L. Hu, Phys. Rev. D **78**, 125025 (2008).
 - [11] S.-Y. Lin and B. L. Hu, Phys. Rev. D **81**, 045019 (2010).
 - [12] A. Raval, B. L. Hu and D. Koks, Phys. Rev. D **55**, 4795 (1997).
 - [13] B. L. Hu, Philip R. Johnson, *Beyond Unruh Effect: Nonequilibrium Quantum Dynamics of Moving Charges*, Invited Talk at the Capri Workshop on Quantum aspects of Beam Physics, Oct. 2000. Proceedings edited by Pisin Chen (World-Scientific, Singapore, 2001) [quant-ph/0012132].
 - [14] J. S. Bell and J. M. Leinaas, Nucl. Phys. B **212**, 131 (1983); J. S. Bell and J. M. Leinaas, Nucl. Phys. B **284**, 488 (1987); W. G. Unruh, Phys. Rep. **307**, 163 (1998); E. T. Akhmedov, and D. Singleton, Int. J. Mod. Phys. **A22** 4797 (2007); E. T. Akhmedov and D. Singleton, Pisma Zh. Eksp. Teor. Fiz. **86** 702 (2007).
 - [15] B. F. Svaiter and N. F. Svaiter, Phys. Rev. D **46**, 5267 (1992); **47** 4802 (1993).
 - [16] A. Higuchi, G. E. A. Matsas and C. B. Peres, Phys. Rev. D **48**, 3731 (1993).

- [17] L. Sriramkumar and T. Padmanabhan, *Class. Quantum Grav.* **13**, 2061 (1996).
- [18] N. Obadia and R. Parentani, *Phys. Rev. D* **67**, 024021 (2003); **67**, 024022 (2003).
- [19] S. Schilicht, *Class. Quantum Grav.* **21**, 4647 (2004); J. Louko and A. Satz, *Class. Quantum Grav.* **23**, 6321 (2006); P. Langlois, *Annals Phys.* **321**, 2027 (2006).
- [20] N. Obadia and M. Milgrom, *Phys. Rev. D* **75**, 065006 (2007).
- [21] R. Casadio and G. Venturi, *Phys. Lett.* **A252**, 109 (1999).
- [22] D. Kothawala and T. Padmanabhan, *Phys. Lett.* **B 690**, 201 (2010).
- [23] S.-Y. Lin and B. L. Hu, *Phys. Rev. D* **76**, 064008 (2007).
- [24] E. A. Calzetta and B.-L. Hu, *Nonequilibrium Quantum Field Theory* (Cambridge University Press, Cambridge, 2008).
- [25] E. G. Kalnins, *SIAM J. Math. Anal.* **6**, 340 (1975).
- [26] I. Costa, *Rev. Bras. Fis.* **17**, 585 (1987); I. Costa, *J. Math. Phys.* **30**, 888 (1989); I. Costa and N. F. Svaiter, *Rev. Bras. Fis.* **19**, 271 (1989); U. Percoco and V. M. Villalba, *Class. Quantum Grav.* **9**, 307 (1992); V. M. Villalba and J. Mateu, *Phys. Rev. D* **61**, 025007 (1999).
- [27] R. B. Mann and V. M. Villalba, *Phys. Rev. A* **80**, 022305 (2009).
- [28] S.-Y. Lin, R. Behunin and B. L. Hu, “Quantum Twin Paradox: Entanglement is memory-laden” in preparation.
- [29] S.-Y. Lin and B. L. Hu, *Phys. Rev. D* **73**, 124018 (2006).
- [30] N. D. Birrell and P. C. W. Davies, *Quantum Fields in Curved Space* (Cambridge University Press, Cambridge, 1982).
- [31] R. Simon, *Phys. Rev. Lett.* **84**, 2726 (2000); L.-M. Duan, G. Giedke, J. I. Cirac, and P. Zoller, *Phys. Rev. Lett.* **84**, 2722 (2000).
- [32] G. Vidal and R. F. Werner, *Phys. Rev. A* **65**, 032314 (2002).
- [33] J. L. Ball, I. Fuentes-Schuller, and F. P. Schuller, *Physics Letters* **A359**, 550 (2006); G. L. Ver Steeg and N. C. Menicucci, *Phys. Rev. D* **79**, 044027 (2009); I. Fuentes, R. B. Mann, E. Martin-Martinez, and S. Moradi *Phys. Rev. D* **82**, 045030 (2010).
- [34] M. K. Parikh and F. Wilczek, *Phys. Rev. D* **58**, 064011 (1998).
- [35] S. A. Hayward, *Phys. Rev. D* **49**, 6467 (1994).
- [36] A. Ashtekar and B. Krishnan, “Isolated and Dynamical Horizons and Their Applications”, *Living Rev. Relativity* **7**, (2004), 10. URL (cited on 25 July 2010): <http://www.livingreviews.org/lrr-2004-10>
- [37] The event horizon being defined at the infinite future, an assumption of its existence is rather unnatural for a dynamical (time-evolutionary) problem as the boundary condition is set in the future, not in the past, i.e., it is introduced in a teleological way, see, e.g., [34] for pathologies arising from such setups.
- [38] We feel that the approach to problems of this nature based on quantum field theory and statistical mechanics, or nonequilibrium quantum field theory (NEqQFT), is generally more malleable and functional than the geometric approach, which, like the etiquette of the aristocrats, is invariably more elegant but restricted. We hasten to add that in contrast to the NEqQFT approach, there have also been developments along the geometric-spacetime approach to relax the notion of event horizon to more general situations, from a strictly global to a more quasi-local sense, such as the isolated horizon of Hayward, Ashtekar et al [35, 36] but the effects of quantum fields in spacetimes with such constructs have yet to be explored to make comparison with the predictions of the nonequilibrium field theory results of the 90s.
- [39] We applied Simpson’s rule generalized to two dimensions for numerical integrations in this paper. Each square in our lattice has five sampling points: the four vertices in the corner and the center point. Similar to Simpson’s 1/3 rule we assign a 1/12 weighting factor for the value of the integrand at each vertex and a 2/3 factor for the value at the center. The error would be $O(L^4)$ with lattice constant L and would not accumulate because the integrand is oscillating.